

M6P-modified solid lipid nanoparticles loaded with matrine for the treatment of fibrotic liver

Xiaochuan Tan, Yumei Hao, Nai Ma, Yige Yang, Wenzhen Jin, Ya Meng, Chuchu Zhou, Wensheng Zheng and Yujia Zhang

Beijing Key Laboratory of Drug Delivery Technology and Novel Formulation, Institute of Materia Medica, Chinese Academy of Medical Sciences & Peking Union Medical College, Beijing, China

ABSTRACT

Liver fibrosis is a key pathological process shared by the progression of various chronic liver diseases. Treatment of liver fibrosis can effectively block the occurrence and development of hepatic cirrhosis or even carcinoma. Currently, there is no effective drug delivery vehicle for curing liver fibrosis. In this study, we designed matrine (MT)-loaded mannose 6-phosphate (M6P) modified human serum albumin (HSA) conjugated solid lipid nanoparticles (SLN), named M6P-HSA-MT-SLN for treatment of hepatic fibrosis. We demonstrated that M6P-HSA-MT-SLN exhibited controlled and sustained release properties and good stability over 7 days. The drug release experiments showed that M6P-HSA-MT-SLN exhibited slow and controlled drug release characteristics. In addition, M6P-HSA-MT-SLN showed a significant targeted ability to fibrotic liver. Importantly, *in vivo* studies indicated that M6P-HSA-MT-SLN could significantly improve histopathological morphology and inhibit the fibrotic phenotype. In addition, *in vivo* experiments demonstrate that M6P-HSA-MT-SLN could reduce the expression of fibrosis markers and alleviate the damage of liver structure. Hence, the M6P-HSA-MT-SLN provide a promising strategy to deliver therapeutic agents to fibrotic liver to prevent liver fibrosis.

ARTICLE HISTORY

Received 7 November 2022
Revised 16 May 2023
Accepted 20 May 2023

KEYWORDS


Liver fibrosis; matrine;
M6P-HSA-MT-SLN; target
delivery


1. Introduction

The chronic liver disease represents a major cause of morbidity and mortality worldwide (Byass, 2014). A wide spectrum of chronic liver injuries such as viral hepatics, cholestatic liver diseases, alcohol abuse, nonalcoholic steatohepatitis, and nonalcoholic fatty liver disease are the leading causes of chronic hepatics inflammation. These manifestations deregulated the wound healing process in the liver, leading to fibrosis (Bataller & Brenner, 2005). Liver fibrosis is common pathogenesis of many chronic liver injuries, and a significant health problem that can ultimately lead to end-stage cirrhosis and hepatocellular carcinoma. In addition, it is a dynamic pathological condition characterized by excessive extracellular matrix (ECM), especially increasing expression and deposition of collagen type I and fibrous scar formation. The accumulation of ECM distorts the normal liver architecture by forming fibrous scars, and the subsequent replacement of hepatocytes by scar tissue can prevent the physiological functions of the liver, leading to a variety of complications, including portal hypertension and hepatocellular carcinoma, finally resulting in liver failure (Kisseleva & Brenner, 2008). The current clinical practices against liver fibrosis focus on removing the insult that triggered liver damage. Nonetheless,

conventional therapy is not sufficiently effective in the treatment of liver diseases due to inadequate concentration of therapeutic agents delivered to the liver. Despite the increasing understanding of the fibrotic mechanism, there remains an urgent need for the specific delivery of an adequate amount of antifibrotic agents to the liver.

Several cellular sources (hepatocytes, hepatic stellate cells (HSCs), macrophages, and liver sinusoidal endothelial cells) (Bartneck et al., 2014) have been identified as the major player in the development of liver fibrosis in both human and experimental studies. Recent elegant fate-tracing studies revealed that HSCs are dominant fibrogenic effectors, independent of the etiology of the liver damage and other cell types involved in fibrosis; these also act by upregulating the number of HSCs and modulating their phenotype (Mederacke et al., 2013). Mannose 6-phosphate/insulin-like growth factor II (M6P/IGF II) receptors are overexpressed on the surface of HSCs during liver fibrosis. Also, M6P-modified human serum albumin (M6P-HSA) is selective to M6P/IGF II receptor and thus, accumulates in the activated HSCs of the fibrotic liver. The M6P-HSA has been applied as a carrier for several drugs, including pentoxifylline, mycophenolic acid, doxorubicin, and gliotoxin (Greupink et al., 2005; Gonzalo et al., 2006; Greupink et al., 2006; Hagens et al., 2006). Therefore, the M6P-HSA

CONTACT Yujia Zhang  zhyj@imm.ac.cn; Wensheng Zheng  wensheng_zheng@126.com 

 Supplemental data for this article can be accessed online at <https://doi.org/10.1080/10717544.2023.2219432>.

© 2023 The Author(s). Published by Informa UK Limited, trading as Taylor & Francis Group.

This is an Open Access article distributed under the terms of the Creative Commons Attribution-NonCommercial License (<http://creativecommons.org/licenses/by-nc/4.0/>), which permits unrestricted non-commercial use, distribution, and reproduction in any medium, provided the original work is properly cited. The terms on which this article has been published allow the posting of the Accepted Manuscript in a repository by the author(s) or with their consent.

conjugation to SLN can be used as the selective carrier of antifibrotic drugs to improve the efficacy of drugs.

Matrine (MT) is a tetracyclo-quinolizidine alkaloid extracted from the roots of *Sophora flavescens* Aiton. Also, it is extensively used owing to its minimum toxicity and cost-efficiency in clinical practices (Ma et al., 2008; Dai et al., 2009). Great advancement has been achieved in understanding the pharmacological effects of MT, which has been reported to possess a variety of pharmacological effects, such as anti-inflammatory, antitumor, and antiviral (Jiang et al., 2018). In recent years, the anti-fibrosis property of MT is recognized and applied as an inhibitory agent for liver fibrosis (J.P Zhang et al., 2001). These findings suggested that MT is a promising therapeutic molecule in the management of liver fibrosis. Nevertheless, the relatively short plasma half-life and rapid clearance properties make MT difficult to attain effective concentration at the disease site (Feng et al., 2016). To overcome these limitations, it is essential to develop an effective delivery strategy for adequate therapeutic performance and clinical applications.

The application of nanoparticle systems has become a rapidly growing area of interest for the safe delivery of various chronic liver disease drugs. The unique properties of controlled release and enhanced drug content are the biggest advantages. Solid lipid nanoparticles (SLN) are characterized by excellent biocompatibility and have the possibility of incorporating both hydrophilic and hydrophobic drugs as well as genes (Din et al., 2019; Rana et al., 2020; Mirchandani et al., 2021). Many reports have described the application of SLN in enhancing the solubility and bioavailability of hydrophobic drugs (Kong et al., 2013; Yang et al., 2020). For example, Xu and Chen developed docetaxel-loaded SLN to specifically target the Asialoglycoprotein (ASGP) receptors overexpressed on HSCs for the treatment of hepatocellular carcinoma (Xu et al., 2009). Currently, Mahdinloo et al. also constructed vitamin A-modified SLN for the treatment of hepatic fibrosis in rats after encapsulation of butein (Mahdinloo et al., 2022). Therefore, these researches suggest that SLNs have potential value as nanocarriers for lipid-soluble drugs.

In this study, the targeted and biocompatible M6P-HSA was synthesized and assembled to MT-SLN for targeted delivery MT to fibrotic liver. In vivo, the pharmacodynamic, targeting ability, organ distribution, blood biochemical indicators and fibrogenic phenotype of M6P-HSA-MT-SLN was evaluated in carbon tetrachloride (CCl₄)-induced liver fibrosis mice. The results demonstrate that M6P-guided SLN preferentially accumulates in fibrotic livers and can be slowly metabolized. Besides, M6P-HSA-MT-SLN can effectively reduce liver fibrosis factors, reduce inflammatory infiltration and alleviate liver fibrosis in vivo.

2. Materials and methods

2.1. Materials

Glyceryl monostearate and stearic acid were purchased from Beijing Fengli Jingqiu Commerce and Trade Co., Ltd (Beijing, China). Glyceryl behenate was purchased from Guangzhou Tianrun Pharmaceutical Co., Ltd (Guangzhou, China). Egg yolk lecithin and soybean lecithin were purchased from Shanghai

Tywei Co., Ltd (Shanghai, China). Poloxamer 188, Span 85, Tween 80, glycerin, and Brij S10 were obtained from Sigma-Aldrich (ST. Louis, USA). MT and FBS was purchased from Innochem Technology Co., Ltd (Beijing, China). P-nitrophenyl- α -D-mannopyranoside, N-succinimidyl-S-acetylthioacetate (SATA), and phosphatidylethanolamine-PEG-maleimide (DSPE-PEG-MAL) were bought from Shanghai Yiyuan Biological Technology Co., Ltd (Shanghai, China). Human serum albumin was purchased from Tokyo Chemical Industry (Shanghai) Development Co., Ltd (Shanghai, China). Phosphorus oxychloride, palladium 10% on carbon, and thiophosgen were bought from Energy Chemical Technology (Shanghai) Co., Ltd (Shanghai, China). Dialysis bags (2500 kDa cutoff) were purchased from Shanghai Yuanye Biological Technology Co., Ltd (Shanghai, China). Ultrafiltration tubes (3 kDa cutoff) were bought from Merck Millipore (Germany). Acetonitrile, methanol, ethanol, and ethyl acetate were of HPLC grade, and other reagents were of analytical grade.

2.2. Synthesis of M6P-HSA

The M6P-HSA was synthesized and characterized as reported previously (Beljaars et al., 1999) (Figure 1C). Firstly, p-nitrophenyl- α -D-mannopyranoside was phosphorylated by phosphorus oxychloride, and p-nitrophenyl-6-phospho- α -D-mannopyranoside (MW 381) was obtained. Subsequently, the nitro group was reduced with 10% palladium on activated carbon under 1.5 atm of hydrogen for 4h to obtain the p-aminophenyl-6-phospho- α -D-mannopyranoside (pap-M6P, MW 350). Then the p-aminophenyl-6-phospho- α -D-mannopyranoside was coupled to HSA by diazo bond formation to get M6P-HSA. The resulting M6P-HSA was purified and analyzed by Sephadex G-50 gel chromatography to determine its molecular weight. The 6-phosphate-p-nitrophenyl- α -D-mannose, p-aminophenyl- α -D-mannose, 6-phosphate-1-(4-isothiocyanatophenyl)- α -D-mannose and M6P-HSA were purified and verified by mass spectrometry. Unmodified HSA protein was isolated using Superdex 75.

2.3. Optimization of the formulation and preparation method of solid lipid nanoparticles

A series of necessary parameters affecting the properties of solid lipid nanoparticles, such as solid lipid materials, surfactants, preparation process, etc., are screened to ensure that the design of solid lipid nanoparticles meets the specific requirements for the expected product performance. The main purpose of the above parameter optimization is to obtain SLNs with suitable polydispersity index (PDI) < 0.3 and nanoparticle size. The total volume of SLN solution was 50 mL, and the mass of MT was 50 mg, and then the prescription was screened and optimized.

2.3.1. Solid lipid material screening

In order to investigate the effect of lipid material on carrier particle size and PDI during the preparation process, three batches of corresponding nanoparticles were prepared by using stearic acid, glyceryl behenate and glyceryl

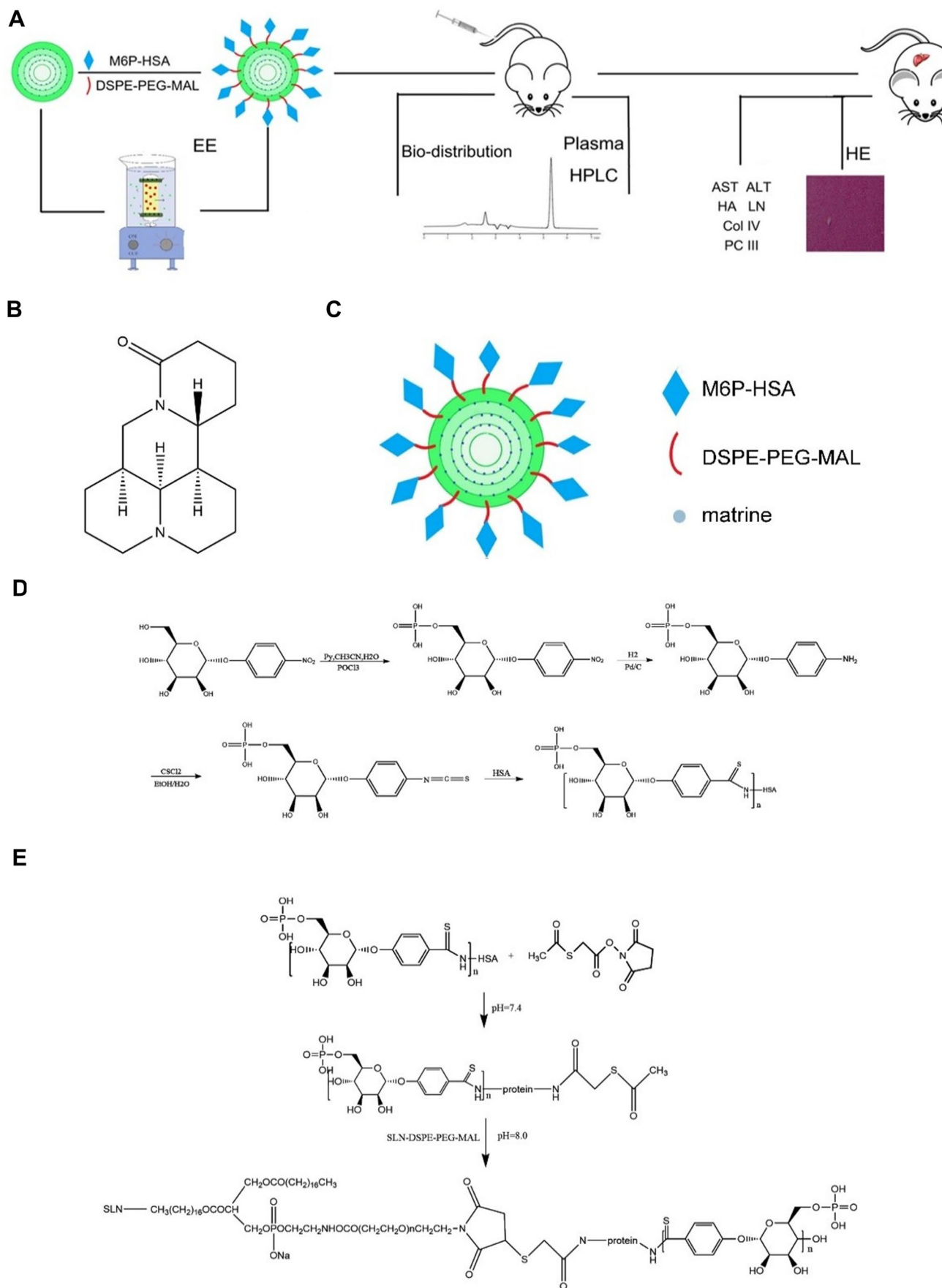


Figure 1. Experimental procedure and synthetic route of M6P-HSA and M6P-HSA-MT-SLN. (A) Experimental procedure outline and timeline. (B) Structure of MT. (C) Structure of M6P-HSA-MT-SLN. (D) Synthesis of M6P-HSA. (E) Connection of M6P-HSA to SLN-DSPE-PEG-MAL.

monostearate respectively, and solidified in ice bath for 24h after preparation. The particle size and PDI of the prepared SLN were investigated.

2.3.2. Surfactants screening

The amount of surfactant and its concentration directly affects the size and degree of polydispersity of the solid lipid dispersion particles. Three batches of corresponding solid lipid nanoparticles were prepared by using common surfactants such as F68, egg yolk lecithin (Lec), granulesten (Gra), glycerol (Gly), Tween-80 (Tween), Brij-S10 (Brij), and Span-85 (Span), and ice bathed after preparation and cured for 24h.

2.3.3. Manufacturing processes screening and optimization

The preparation methods of solid lipid nanoparticles have a great influence on the quality of SLN, including microemulsion method, microemulsion-probe ultrasonic method, thin film ultrasonic dispersion method, etc. In this experiment, three batches of SLN were prepared by microemulsion method, microemulsion-probe ultrasonic method, thin film ultrasonic dispersion method, etc., and then the PDI and particle size of each method were compared.

2.4. Preparation and characterization of MT-SLN and M6P-HSA-MT-SLN

Various methods have been developed to prepare SLN (Rana et al., 2020). Based on the previous screening, this study established a microemulsion-probe ultrasound method for the preparation of SLN. MT loaded SLN (MT-SLN) was prepared as follows: Firstly, MT was added into the ethanol solution containing phospholipid and the obtained mixture was stirred to form a complex. After the ethanol was evaporated, glyceryl monostearate was added and melted at 70°C. Stirring was facilitated at 400 rpm for 30 min to obtain the homogenous mixture of MT in the lipid phase. The aqueous phase (100 mL) was prepared by solubilizing the poloxamer 188 in water and heating to 70°C. The aqueous phase was added to the lipid phase, and stirring was continued at 70°C. After 30 min, the hot emulsion was allowed to probe ultrasound with 250W for 10 min to obtain transparent and light blue milky MT-SLN solution. The solution was cooled at 4°C overnight to maintain the form of SLN.

The M6P-HSA-modified MT-SLN (M6P-HSA-MT-SLN) were prepared by following steps (Figure 1D). Firstly, the synthetic M6P-HSA was incubated with S-acetylthioglycolic acid N-hydroxysuccinimide ester (SATA) in borate buffer (pH = 7.4) for 4h to prepared M6P-HSA-SATA, and the product was lyophilized. Secondly, maleimide modified MT-SLN was prepared according to the preparation method of MT-SLN, and the same amount of lecithin in the lipid composition was replaced by DSPE-PEG-MAL (20 mg). Finally, M6P-HSA-SATA was added to maleimide modified MT-SLN solution and stirred for 5h to obtain M6P-HSA-MT-SLN.

Size and zeta potential were measured by dynamic light scattering (DLS) using a Zetasizer (Malvern Nano ZSP, Malvern,

UK) at room temperature. Before measurements, the instrument was calibrated using a standard sample (Din et al., 2015).

2.5. Measurement of encapsulation efficiency and drug loading efficiency

Encapsulation efficiency (EE) is crucial for evaluating the quality of the carrier and was measured as described previously (Zhang et al., 2019). Briefly, 0.3 mL carrier solution was added into the inner of the ultrafiltration tube and centrifugated at 8000 rpm for 30 min. The MT solution in water was leaked into the external tube, and drug encapsulated in the core of carrier, larger in size was blocked in the internal tube. The amount of the non-encapsulated drug was measured, and the EE was determined using the following equation:

$$EE(\%) = \frac{\text{weight of the drug encapsulated in carriers}}{\text{weight of drug added}} \times 100\%$$

The ultrafiltration tube was pre-saturated with distilled water, and the recovery rate was measured. An HPLC method was established to measure the concentration of MT. The HPLC system consisted of a solvent delivery pump (1100, Agilent Technologies, Japan) and a DAD detector (1100, Agilent technologies). The chromatographic column consisted of Diamonsil® Plus C-18 (250 mm × 4.6 mm, 5 μm), mobile phase of 90% 0.025 mol/L potassium dihydrogen phosphate solution and 10% acetonitrile solution, detection wavelength 210 nm, column temperature 30°C, velocity of 1 mL/min, and sampling amount 20 μL. Also, the linearity, specificity, intra- and inter-day variabilities, and recovery of HPLC methods were quantitated for the samples.

2.6. In vitro release kinetics of MT from MT-SLN and M6P-HSA-MT-SLN

Briefly, 0.5 mL ($n=3$) of MT containing SLN was sealed in a dialysis bag. These bags were submerged in 50 mL of release media (simulated serum, pH 7.4+20% fetal bovine serum (FBS)), with constant stirring at 200 rpm at 37°C. At predetermined time intervals, 0.5 mL of release medium was sampled and replenished by an equivalent volume of fresh medium. The samples were filtered through a 0.22 μm syringe membrane filter. The concentration of the released MT was analyzed by the HPLC method.

2.7. Stability study of MT-SLN and M6P-HSA-MT-SLN

Stability is a critical parameter to evaluate the quality of the carrier (Batool et al., 2021; Xing et al., 2021). In this study, the size and EE were measured and compared before and after storage to assess the stability of the carrier.

2.8. Selection of methods for constructing liver fibrosis models

The liver fibrosis model was established and evaluated using C57BL/6 mice. The chronic liver injury was induced by CCl₄, as described previously (Sakaida et al., 2004). The

concentration and injection dose of carbon tetrachloride, as well as whether it is combined with ethanol, and modeling time have a great influence on the degree of fibrosis in the liver fibrosis model. The above factors were investigated and optimized, and the changes of liver fibrosis markers AST and ALT in serum were used as indicators to screen the method for building a mouse liver fibrosis model.

2.8.1. Selection of modeling time

All of 48 C57BL mice were injected with 30% CCl₄, and blood was collected from the retro-orbital venous plexus of mice at 1, 2, 3, 4, 5, 6, 7, and 8 weeks after modeling to determine the concentration of ALT and AST.

2.8.2. Selection of CCl₄ concentration

The mice were randomly divided into 4 groups (6 of each group) and were injected intraperitoneally with 0%, 20%, 30%, and 40% CCl₄ oil solution, twice a week. The serum ALT and AST concentrations were detected after the mice were sacrificed 4 weeks later.

2.8.3. Selection of CCl₄ volume

The mice were randomly divided into 4 groups (6 of each group) and injected with 0, 0.1, 0.15 and 0.2 ml of 30% CCl₄ oil solution respectively, twice a week. The serum ALT and AST concentrations were detected after the mice were sacrificed 4 weeks later.

2.8.4. Selection whether to feed ethanol

The mice were randomly divided into 3 groups (6 of each group), and 30% CCl₄ oil solution was injected intraperitoneally, twice a week. Normal group: healthy mice without CCl₄ and drinking water; without ethanol group: mice was injected with 30% CCl₄, and given drinking water; with ethanol group: mice was injected with 30% CCl₄ and given 8% ethanol in water. The serum ALT, AST, HA, LN, PCIII and Col IV concentrations were detected after the mice were sacrificed 8 weeks later.

2.9. M6P-HSA-MT-SLN treatment of CCl₄-induced liver fibrosis in mice

C57BL/6 mice (18–20 g) were purchased from Beijing Vital River Laboratory Animal Technology Co., Ltd (Beijing, China). The liver fibrosis mouse model was constructed according to the modeling method screened. Liver fibrosis was induced in healthy male C57BL/6 mice by intraperitoneal injection of 10 mL/kg CCl₄ (30% in olive oil), two times a week for 4 weeks. The mice were administered an 8% ethanol solution as a supplement of water during the period of model establishment.

A total of 180 C57BL mice were randomly divided into five groups (each group of 32 mice) and administered the corresponding drugs: control group (healthy mice without CCl₄), Model group (CCl₄ but no drug), MT-solution group (CCl₄ with free MT solution), MT-SLN group (CCl₄ with MT-SLN), and M6P-HSA-MT-SLN group (CCl₄ with M6P-HSA-MT-SLN). Mice were injected intravenously with corresponding MT

solution (20 mg/kg) via the tail three times a week. The serum and liver samples of 8 mice in each group were collected once a week. And blood samples were collected from each mouse at the end of 4 weeks, then the level of AST, ALT, HA, LN, PC III, and Col IV in serum were measured. The body weight was also measured and recorded. The level of liver fibrosis biomarkers (AST, ALT, HA, LN, PC III, and Col IV) in the serum of each mouse was compared before and after drug administration using the ELISA kits. The standard curve was produced according to the operation instructions, and the concentration of biomarkers was determined according to the standard curve. Hematoxylin-eosin (H&E), Masson staining, and Sirius Red staining were utilized to measure the degree of liver fibrosis in mice to calculate the effect of the M6P-HSA-MT-SLN. The image analysis software Pro-Plus 7.0 was used to estimate the proportion of inflammation/necrotic lesion involvement area in the total liver tissue section. And the IHC of α -SMA and collagen I of liver sections was used to investigate antifibrotic effect on hepatic stellate cells of different MT formulations.

2.10. Biodistribution of M6P-HSA-MT-SLN in rats

Male Sprague–Dawley rats (180–200 g) were purchased from Beijing Vital River Laboratory Animal Technology Co., Ltd (Beijing, China). The following studies were carried out in compliance with the regulations and guidelines of the Laboratories' Institutional Animal Care and Use Committee of the Chinese Academy of Medical Sciences and according to the guidelines and ethics of the Chinese Council on Animal Care.

A total of 90 CCl₄-induced SD rats (Li et al., 2020) were randomized into three groups (each group of 30 rats) and administered free MT solution, MT-SLN and M6P-HSA-MT-SLN at a dose of 50 mg/kg via tail, respectively. Five rats in each group were sacrificed at 0.5, 1, 2, 4, 8, and 12 h respectively, and the main organs (heart, liver, spleen, lung, kidney) were collected and stored at –80 °C for analysis. Before analysis, the organs were thawed, and 100 mg samples were homogenized in 0.9 mL precooled saline (4 °C). The distribution of MT in the tissues was measured and compared.

2.11. In vivo pharmacokinetic study

A total of 18 healthy male SD rats (200 ± 10 g) were randomly divided into groups A, B and C (each group of 6). Each group was given 50 mg/kg MT solution, MT-SLN and M6P-HSA-MT-SLN, respectively. SD rats were fasted for 12 h and fed drinking water prior to administration of MT formulations. Blood samples were collected at pre-determined intervals (0, 5, 30 minutes, 1, 2, 4, 6, 8, 10, 12 hours after injection). Plasma samples were obtained by centrifugation of blood samples at 5000 rpm for 15 minutes at 4 °C and stored at –80 °C until further analysis. Methanol was selected to remove proteins from the plasma. The mixture of methanol and plasma samples was vortexed for 5 minutes at room temperature. After centrifugation at 12,000 rpm for 10 minutes, the upper layer of the mixture containing MT was collected and evaporated under N₂ at 37 °C. The

resulting solid was dissolved in 100 μ L of 50% methanol solution and 5 μ L of supernatant was selected for injection into the LC-MS² system. Various pharmacokinetic parameters were calculated as reported. Various pharmacokinetic parameters were calculated according to the report.

2.12. Statistical analysis

All experimental data are expressed as mean \pm standard deviation. The statistically significant difference between the two groups was determined by a two-tailed *t*-test, while that between multiple groups was analyzed by analysis of variance (ANOVA), followed by Bonferroni's posthoc *t*-test. $P < 0.05$ was considered as statistically significant and denoted as * ($P < 0.05$), ** ($P < 0.01$), # (not significant).

3. Results and discussion

3.1. Synthesis and characterization of M6P-HSA

As previously described, 6-Phosphate-1-(4-isothiocyanatophenyl)- α -D-mannanose was synthesized from *p*-nitrophenyl- α -D-mannopyranose as the starting product. Then the 6-Phosphate-1-(4-isothiocyanatophenyl)- α -D-mannanose was coupled with human serum albumin to obtain M6P-HSA. The synthetic route of M6P-HSA was shown in Figure 1(C)–(D). The molecular weight of 6-phosphate-*p*-nitrophenyl- α -D-mannose, *p*-aminophenyl- α -D-mannose and 6-phosphate-1-(4-isothiocyanatophenyl)- α -D-mannose were evaluated by Mass spectrometry technology, as shown in Figure 2(A)–(C). The mass spectrometry results showed that *p*-aminophenyl- α -D-mannanose with a molecular weight of 351 was obtained by hydrogenation reduction of 6-phosphoric acid-*p*

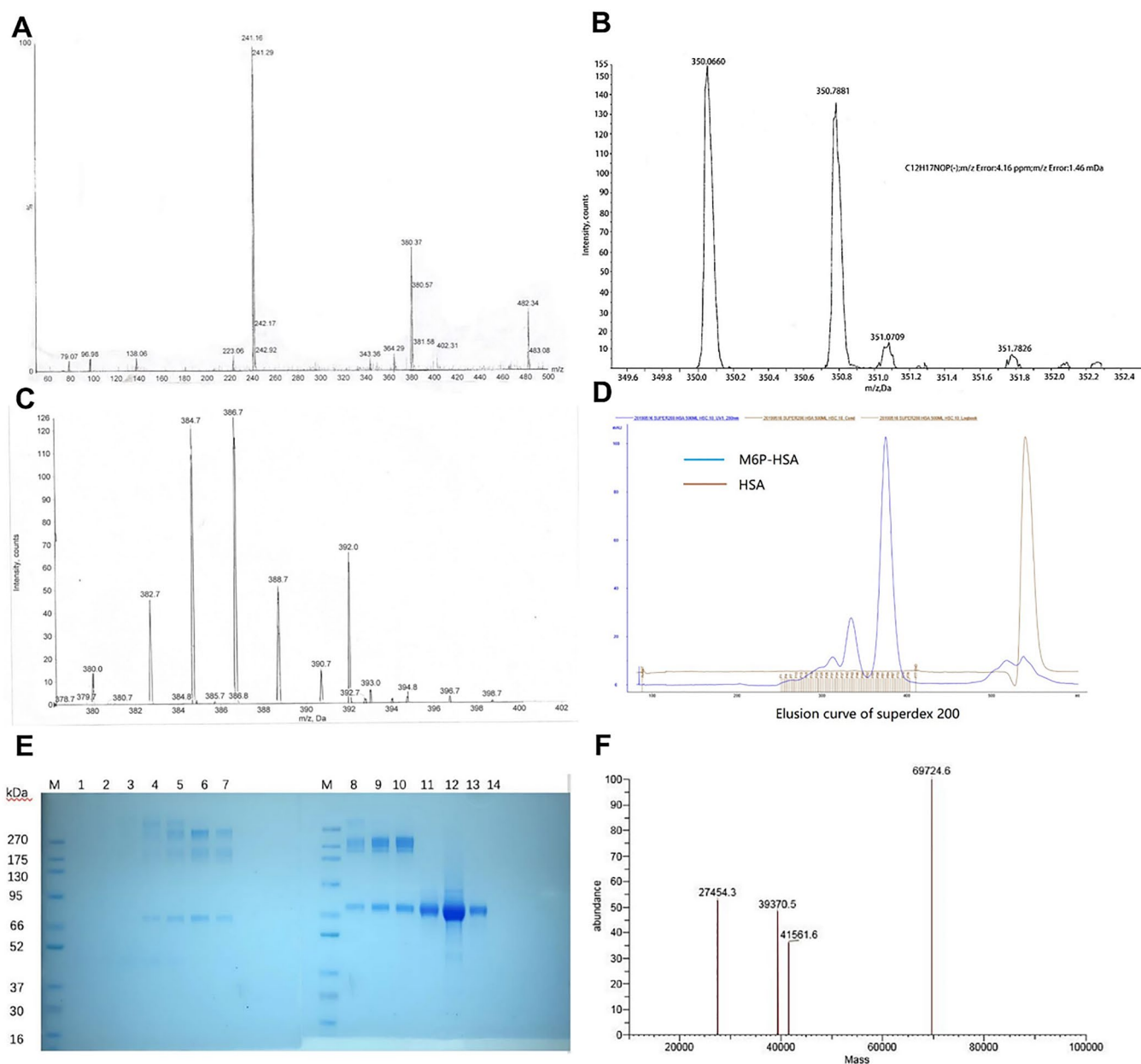


Figure 2. Characterization of M6P-HSA and its related Intermediates. (A) Mass spectrogram of 6-phosphate-*p*-nitrophenyl- α -D-mannose. (B) Mass spectrogram of *p*-aminophenyl- α -D-mannose. (C) Mass spectrogram of 6-phosphate-1-(4-isothiocyanatophenyl)- α -D-mannose. (D) Elution curve of superdex 75 of M6P-HSA and HSA. (E) SDS-PAGE results of M6P-HSA. (F) Mass spectrum of M6P-HSA.

-nitrophenyl- α -D-mannose. After the reaction of p-aminophenyl- α -D-mannanose with thiophosgene, a dark brown 6-phosphate-1-(4-isothiocyanate phenol)- α -D-mannanose with a molecular weight of 393 was obtained. The ratio of mannose to human serum protein was adjusted to obtain mannose human serum protein modified to different degrees. As shown by the elution curve, human serum proteins were modified to different degrees, among which the HSA with high modification rate were few and with low modification rate were more (Figure 2D). SDS polyacrylamide gel results showed that the modified M6P-HSA band appeared at about 70kDa with extremely high intensity, suggesting that the molecular weight of the obtained target was about 70kDa (Figure 2E). The molecular weight of M6P-HSA protein was determined by mass spectrometry, and it was found that the molecular weight of the coupled protein was 69kDa, which was 3kDa higher than that of the unmodified protein (Figure 2F). The molecular weight of a single M6P is about 363, so there are about 10 M6P attached to one HSA molecule, which is close to the ratio of mannose to human serum protein in the product target measured before.

3.2. Selection of lipids and surfactant

In this study, the solid lipid nanoparticles (SLN) were selected due to their biocompatibility, ease of encapsulation, and surface modification ability. SLN constitute the lipid-based nanocarrier family. These were first utilized in the early 1990s as an efficient and nontoxic drug carrier system made up of natural lipids that are solid at body temperature (Kumar & Randhawa, 2013a). Typically, the carrier is prepared from physiological lipids and biocompatible surfactants, which render the SLN well-tolerated in the living systems; therefore, no acute toxic effects are expected from the degradation of

the SLN (Kumar & Randhawa, 2013b). It has been proved that the choice of lipids, emulsifiers, and their concentrations affected the stability and storage ability of SLN (Kumar & Randhawa, 2013b; Ban et al., 2014). The size of the ideal system was expected to be 100–200 nm, as well as a narrow polydispersity index (PDI). First of all, the total volume of SLN solution was 50 mL and the mass of MT was 50 mg. Then the prescription was screened and optimized.

The type and amount of solid lipids were determined by particle size and PDI results. The results showed that the PDI of nanoparticles prepared by using glyceryl monostearate (GM), glyceryl behenate (GB) and stearic acid (SA) were all between 0.2 and 0.3 (Figure 3A). Therefore, it is necessary to further screen suitable lipid species by the size of the particle size. The results of DLS showed that the nanoparticles prepared using GM had a particle size of 90–100 nm, GB was 170–180 nm, and SA was 1200–1300 nm (Figure 3A). Therefore, GM was selected as the solid lipid material for the preparation of SLN in this study. Subsequently, the amount of GM was examined. Briefly, 100, 150, 200, and 150 mg of GM were weighed to prepare SLN and solidified in an ice bath for 24 h after preparation. The particle size and PDI of each group of nanoparticles were determined. From Figure 3(B) (black column), it can be found that with the increase of GM dosage, the size range of nanoparticles changes less. However, from the PDI results (Figure 3B, white column), the PDI of GM showed a minimum value at the dosage of 150 mg. Therefore, GM was finally selected as the lipid material in this experiment, and its dosage was 150 mg.

The surfactants F68, egg yolk lecithin (Lec), granulesten (Gra), glycerol (Gly), tween-80 (Tween), Brij-S10 (Brij), and Span-85 were screened. Figure 3(C) (black column) showed that the particle size distribution of the carriers prepared

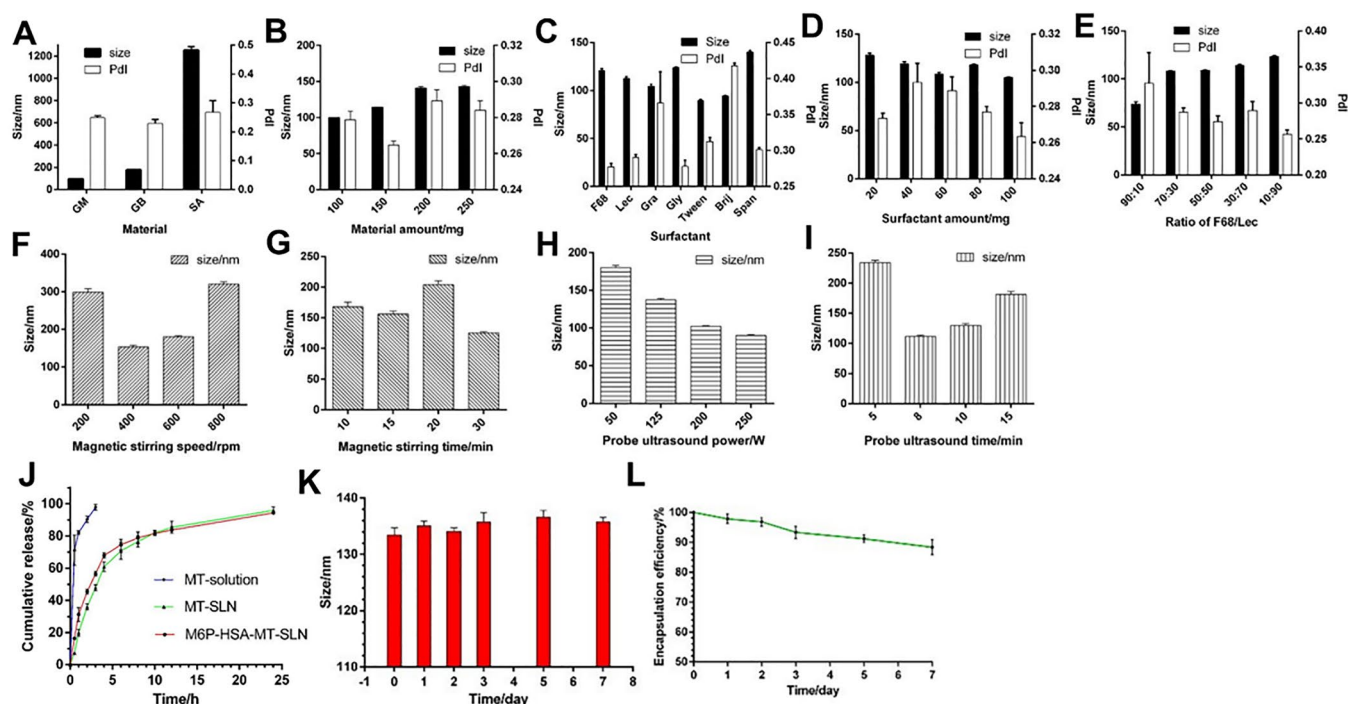


Figure 3. Characterization of M6P-HSA-MT-SLN. (A-I) Optimization of prescription and preparation method of MT-SLN. (J) the in vitro release Profiles of Matrine (MT), MT-SLN, and M6P-HSA-MT-SLN. (K-L) The size and encapsulation efficiency stability study of M6P-HSA-MT-SLN.

by different surfactants was between 90 and 150 nm, which could basically achieve passive targeting. However, the PDI of the above surfactants were quite different. From the Figure 3(C) (white column), the PDI values of the solid lipid nanoparticles prepared from F68, Lec, and Gly were smaller, indicating that the particles size distribution of the SLN prepared by them was uniform. Considering the excellent biocompatibility of F68 and Lec, so they will be used in combination as surfactants for the preparation of SLN in this study. Subsequently, the mass ratio of F68 and Lec was fixed at 1:1, and the particle size and PDI of SLNs with a total mass of 20, 40, 60, 80, and 100 mg were investigated. As we can see in Figure 3(D), it was found that the particle size change was small, while the PDI value was greatly affected by the amount of surfactant. The PDI values were smaller at 20 and 100 mg of surfactant. However, the increase in the amount of surfactant can make the preparation of solid lipid nanoparticles easier and more stable, so 100 mg was chosen as the amount of surfactant. Then the mass ratio of F68/LEC was set to 1:9, 2:8, 3:7, 4:6, 5:5, 6:4, 7:3, the total mass of both was 100 mg. Subsequently, SLN was prepared and measured the particle size and PDI of each group of nanoparticles. Figure 3(E) showed that as the mass of Lec increased, the particle size of SLN gradually increased, while that of PDI gradually decreased. MT is a compound with excellent lipo-solubility and water solubility that makes it difficult to be encapsulated in the core of the nanoparticle. It has been proved that the increased lipo-solubility of the drug improves the EE in the carrier. Interestingly, the usage of Lec increased the lipo-solubility of drug. In this study, the mixture of MT and lecithin was formed before encapsulation in the lipid, thereby increasing the amount of the drug in the core of SLN.

In above, factors affecting carrier formation, including formulation and processing techniques, have been assessed previously herein to obtain suitable drug delivery formulations. In addition to selecting and optimizing the type and amount of solid lipids, the type, quantity and proportion of solid lipids used were also screened. On the basis of the single-element experimental results, a four-factor three-level experiment was designed and carried out to determine the optimal formula. The final prescription decision was as follows: GM/F68/Lec/MT = 150/10/90/50.

3.3. Selection of process parameters for microemulsion-probe ultrasonic method

The process parameters affecting the formation of the carrier were also evaluated and optimized. In this study, the microemulsion-probe ultrasound method was employed to build the nanoparticles. Therefore, to determine the optimal preparation method, we compared the effects of magnetic stirring speed, magnetic stirring time, probe ultrasonic power and ultrasonic time on the particle size of SLN. Figure 3(F) shows that the prepared nanoparticles have the smallest particle size when the rotation speed is 400 rpm. The results showed that the particle size of SLN was less than 200 nm when the stirring time was 10, 15 and 30 min, and the particle size of SLN was close to 100 nm when the magnetic

stirring time was 30 min (Figure 3G). As we can see from the Figure 3(H), it showed that with the increase of ultrasonic power, the size of SLN gradually decreased. In addition, from the appearance of the solution, it was found that the SLN solution obtained by high-power ultrasound was clear and transparent, while the solution obtained by low-power ultrasound appeared milky white instead of light blue opalescence. Investigating the duration of ultrasound, it was found that the size was larger than 200 nm at 5 min of ultrasound, and then the particle size became larger with the increase of ultrasound time (Figure 3I). The increase of ultrasonic time is conducive to the uniform dispersion of solid lipid materials and the formation of solid lipid nanoparticles, but too long ultrasonic time will destroy the structure of the formed carrier, resulting in the aggregation of solid lipid materials and the increase of nanoparticle size. Therefore, the sonication time was determined to be 8 min. In conclusion, the final preparation method of SLN was stirring at a speed of 400 rpm for 30 min and an ultrasonic power of 250W for 8 min.

3.4. Preparation and characterization of MT-SLN and M6P-HSA-MT-SLN

MT-SLN and M6P-HSA-MT-SLN were prepared by microemulsion-probe sonication. M6P-HSA was bound to Maleimide-modified MT-SLN to obtain M6P-HAS-MT-SLN (Figure 1D). Table 1 showed the average size (Z-Ave), PDI, Zeta potential and encapsulation efficiency of Blank-SLN, MT-SLN and M6P-HSA-MT-SLN. The diameter of the M6P-HSA-MT-SLN was 139.3 ± 2.5 nm, and that of the non-modified MT-SLN was 120.6 ± 3.9 nm. These results confirmed that the conjugation of M6P-HSA increased the particle size to a small degree. Similarly, all the nanoparticles exhibited a similar negative zeta potential around -45 mV. Particle size, PDI, and zeta potential are critical factors for nanocarriers, which influenced the distribution of particles (Jin et al., 2007). An appropriate particle size could prolong the circulation time of the carrier in the blood and improve the bioavailability. The zeta potential is a key factor affecting the stability of the particle system. It has been proved that the higher the absolute value of the zeta potential, the more stable the carrier (Xu et al., 2011). Together, results revealed that the M6P-HSA-MT-SLN was an optimal drug carrier.

Stability is a major index for drug carriers. The changes in the size and encapsulation efficiency (EE) were measured to evaluate the storage stability for this nanocarrier. The size of the nanocarrier suspensions before and after storage at 4°C was compared. Small particle size change was observed after 1 week storage of nanoparticles at 4°C (Figure 3K), and the drug encapsulated in the SLN was stable with high EE

Table 1. Parameters of different formulations.

Parameters	Blank SLN	MT-SLN	M6P-HSA-MT-SLN
Z-Ave (nm)	116.7 ± 2.6	120.6 ± 3.9	139.3 ± 2.5
PDI	0.224	0.219	0.209
Zeta potential (mV)	-43	-44.6	-45.1
EE%		65.7	59.6

(Figure 3L), indicating that the SLN has excellent stability at 4°C for 1 week.

3.5. In vitro release of MT from MT-SLN and M6P-HSA-MT-SLN

The in vitro release behavior of MT was analyzed by the dialysis method in simulated serum in order to forecast the putative in vivo behavior and obtain a proper nanocarrier for liver fibrosis treatment. MT showed different release behaviors because of the different formulations, indicating that the release behaviors were affected by the SLN. As shown in Figure 3(J), the MT was rapidly released in free MT solution. 90% of the free MT drug solution was released into the medium in approximately 1 hour, suggesting a rapid release after injection into the body, possibly resulting in unsatisfactory retention times. On the contrary, the release of MT from MT-SLN and MT-M6P-HSA-SLN exhibited a biphasic pattern of a slow and sustained release. Figure 3(J) showed that the MT-SLN and M6P-HSA-MT-SLN obtained over 80% of drug release after 10h. The sustained release of the MT in SLN and target SLN may be due to the interactions between the phospholipid and the homogenous entrapment of the drug (Rahman et al., 2013). The release profile showed that MT-SLN and M6P-HSA-MT-SLN formulation could release MT at a slow and sustained rate, and the anti-fibrosis drug could maintain a potential application in enhancing the bioavailability and continuous efficiency. The prolonged release of MT may provide an enhanced therapeutic effect against hepatic fibrosis in vivo. Therefore, SLN can serve as an effective carrier system for MT to improve the release properties of MT and ensure that more MT is available to HSCs in liver.

3.6. Model building method screening

The carrier was designed to increase the retention amount of the drug in the liver, allowing an improved effect against fibrosis. The fibrosis mouse model induced by CCl₄ is characterized by the proliferation and differentiation of hepatic stellate cells. In this study, a mouse model of liver fibrosis was established by intraperitoneal injection of CCl₄ oil solution combined with drinking ethanol aqueous solution. The modeling time, the concentration of CCl₄, the volume of CCl₄, and whether to drink alcohol were investigated to determine the best animal modeling method.

3.6.1. Selection of modeling time

First, mice were intraperitoneally injected with 30% CCl₄ for 8 weeks, and the serum ALT and AST levels of mice were detected after each week. The time of modeling was investigated, and the results showed that the levels of ALT and AST at four weeks of modeling were significantly higher than those of mice without modeling at 0 weeks (Figure 4J). The mice showed reduced food intake, weight loss, listlessness, and dull hair. Four weeks later, the results showed that the levels of ALT and AST did not change much. Considering that some animals died after four weeks of injection, 4 weeks was chosen as the modeling time.

3.6.2. Selection of CCl₄ concentration

The serum ALT and AST levels of the mice were detected, and it was found that the 20%, 30% and 40% CCl₄ groups were greatly increased compared with the normal mice, suggesting that the liver fibrosis indexes of the mice were increased. It was further found that ALT and AST were lowest in the 20% CCl₄ group, indicating less fibrosis in this group (Figure 4A,B). The 30% and 40% CCl₄ groups had heavier levels, but there was no significant difference between the two groups (Figure 4A,B). In addition, at the end of the modeling, the mice in each group were dull and in poor spirits. Some mice in the 40% CCl₄ group died, but not in the 20% and 30% 40% groups. Therefore, a concentration of 30% CCl₄ was selected for the liver fibrosis mouse model.

3.6.3. Selection of CCl₄ volume

The volume of 30% CCl₄ was investigated, and the effects of different volumes of CCl₄ on serum AST and ALT in mice were compared. After 4 weeks of 30% CCl₄ injection, the mice in the 0.1 mL group was better, while the response of mice in the 0.15 mL and 0.2 mL groups was sluggish. The ALT level showed that the 0.2 mL group and the 0.15 mL group were higher than the 0.1 mL group, and the AST level showed that the 0.2 mL group was higher than the 0.1 mL group (Figure 4C,D). Taking into account comprehensively, 0.2 mL CCl₄ oil solution was selected to construct the liver fibrosis mouse model.

3.6.4. Selection whether to feed ethanol

Finally, it was investigated whether the combined consumption of ethanol further induced liver fibrosis. Figure 4(E)–(J) showed that the levels of liver fibrosis indicators (ALT, AST, HA) in mice drinking ethanol water solution group were higher than those in pure water drinking group. Therefore, 8% ethanol in water was fed to mice to induce liver fibrosis.

3.7. M6P-HSA-MT-SLN alleviates the CCl₄-induced liver fibrosis in vivo

In this study, the fibrosis model was established with C57 mice by intraperitoneal injection of 30% CCl₄ accompanied by drinking 8% ethanol solution, for 4 weeks. Before the functionalized nanoparticles were injected intravenously, hemolysis experiments were performed to investigate the in vivo biocompatibility of the different MT formulations (Song et al., 2023). Figure S1 reveals that free MT solution, MT-SLN and M6P-HSA-MT-SLN exhibited no significant hemolysis (less than 5%) at different dilution concentrations (stock solution, 2-fold dilution).

Concentrations of fibrotic biomarkers such as AST, ALT, HA, LN, Col IV, and PC III were measured in fibrotic mice before and after MT treatment to assess the remission of fibrosis. After 1 week of treatment, the concentration of liver fibrosis factor indexes in the serum of the model group increased, and the free MT solution group, the MT-SLN group and the M6P-HSA-MT-SLN group all decreased slightly (Figure 5A–F). There were no significant differences in the reduction of fibrotic factors among the three groups, suggesting that the designed particles did not have much advantage over

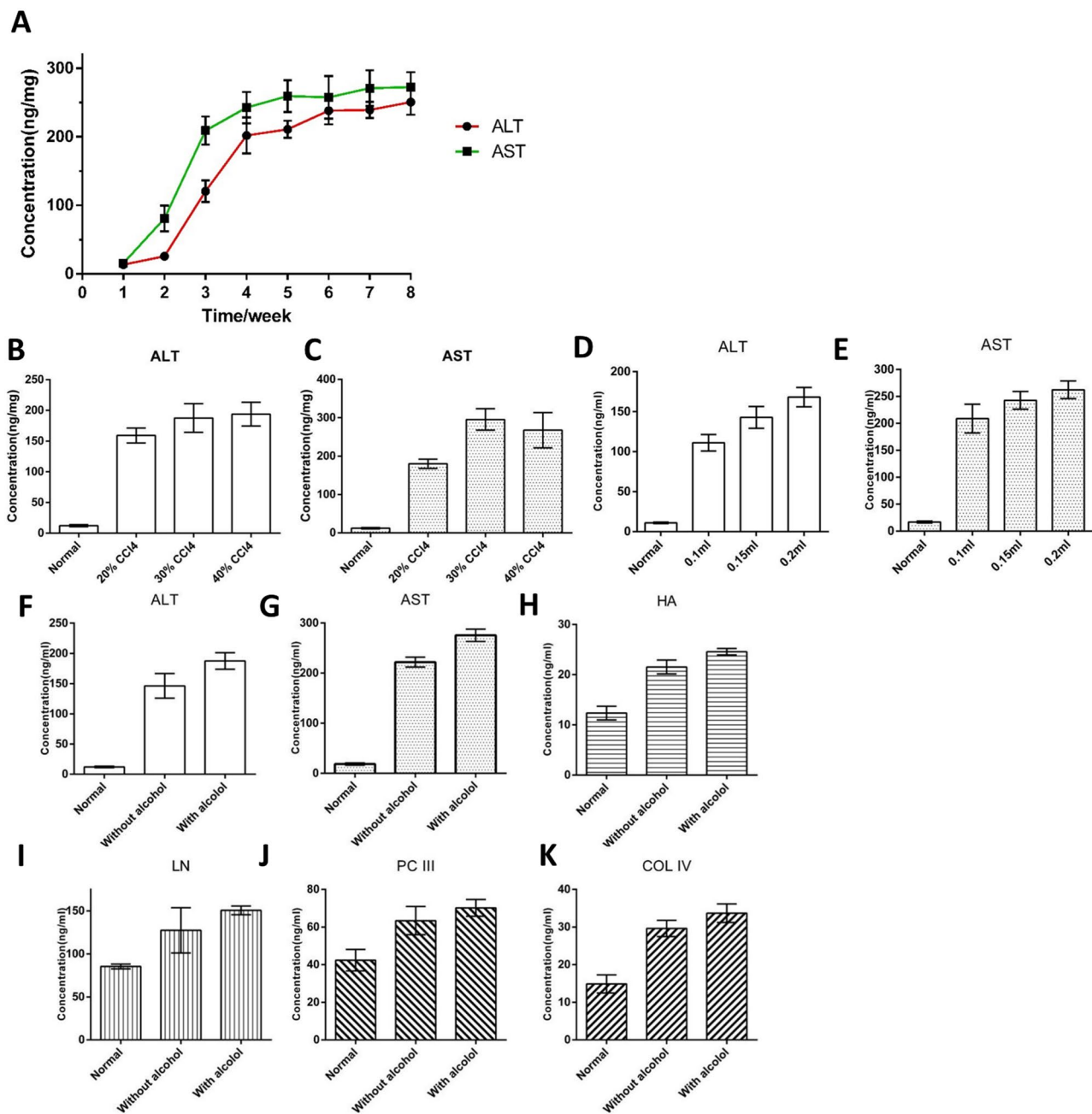


Figure 4. Optimization of carbon tetrachloride-induced liver fibrosis model. (A) ALT and AST results for modeling time Selection. (B-C) ALT and AST results of CCl₄ concentration selection. (D-E) ALT and AST results of CCl₄ volume selection. (F-K) ALT, AST, HA, LN, PCIII and Col IV results of whether to feed ethanol.

other particles in the short term. Furthermore, it was shown that the M6P-HSA-MT-SLN had a great advantage when the treatment progressed to 4 weeks. Briefly, MT-SLN and free MT solution showed good efficacy, while mice administered M6P-HSA-MT-SLN showed the greatest reduction in biomarker levels, suggesting that targeting ability of M6P enhances the therapeutic effect of MT. The significant difference in therapeutic efficacy between MT-SLN and M6P-HSA-MT-SLN was attributed to the specific targeting ability of M6P-modified SLN on hepatic stellate cells, which are activated in the fibrotic liver. Consistently, Luk et al. prepared M6P-modified HSA-GA, which could enrich in activated HSC and attenuated collagen deposition in the BDL-injured liver (Luk et al., 2007). Previous study has also shown that M6P-modified albumin

is efficiently taken up by HSCs in fibrotic livers, suggesting that M6P could be used as a selective ligand for the delivery of antifibrotic drugs to HSCs (Beljaars et al., 1999).

H&E staining further confirmed the excellence of MT-SLN and M6P-HSA-MT-SLN in each week of treatment. The degree (Figure 5G) of fibrosis was scored according to H&E staining (Figure 6A), and the higher the score, the more severe the fibrosis. H&E score: the proportion of inflammatory/necrotic lesion area to the whole H&E slice staining area is calculated using the software Image Pro-Plus and then scored according to the Table S1. The score results showed that the model group had higher scores than the three treatment groups, indicating that fibrosis persisted without treatment. Mice in the free MT, MT-SLN and M6P-HSA-MT-SLN groups had lower scores than

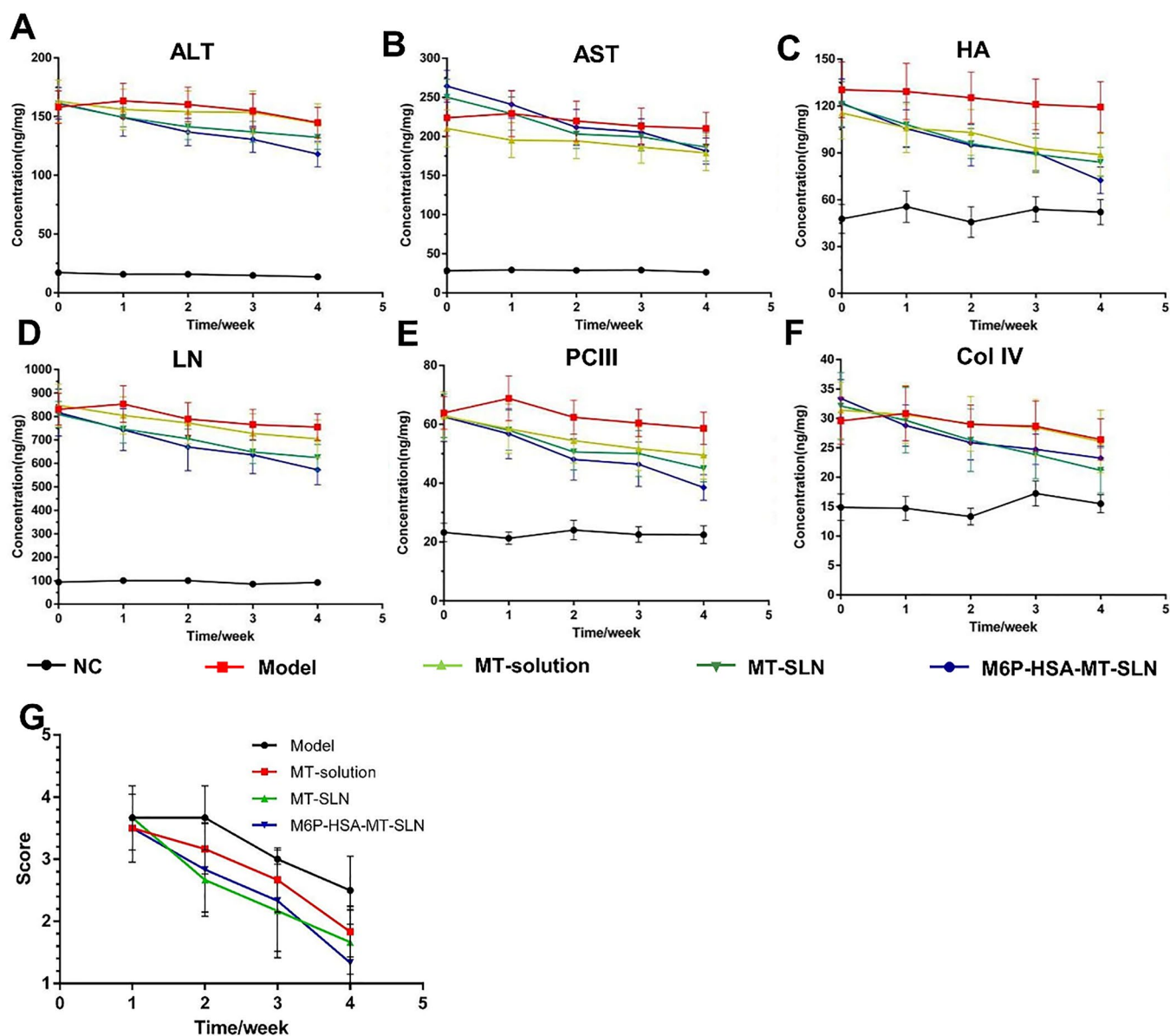


Figure 5. The treatment of MT-SLN and M6P-HSA-MT-SLN in CCl_4 -induced fibrotic mice. (A–F) Serum ALT (alanine aminotransferase), AST (aspartate aminotransferase), HA (hyaluronic acid), LN (laminin), PC III (procollagen type III), and COL IV (collagen type IV) levels in fibrotic mice treated for 1–4 weeks. (G) Analysis of H&E staining results in fibrotic mice treated for 1–4 weeks.

model group, and the M6P-HSA-MT-SLN group had the lowest score, representing the best treatment effect. These results suggest that SLN-encapsulated MT can more easily enter the fibrotic liver to play an effective anti-fibrotic therapeutic role.

Figure 6A shows images of H&E, Masson and Sirius Red staining of liver fibrosis mice at the end of the fourth week of administration. The results revealed that the liver tissue in the model group exhibited severe inflammatory infiltration, collagen deposition and central necrosis of the liver lobules. As shown in Figure 6(A), the MT-SLN and M6P-HSA-MT-SLN groups were found to exhibit intact liver structure as well as minimal collagen deposition, indicating that MT-SLN and M6P-HSA-MT-SLN could protect the CCl_4 -induced mice from liver fibrosis. Furthermore, M6P-HSA-MT-SLN exhibited minimal inflammatory infiltration, disruption of liver structure and collagen deposition. However, similar treatment with free MT resulted in little

improvement in liver structure and a slight reduction in collagen deposition. The analysis of the percentage of H&E, Masson and Sirius Red staining area in the control and different treatment groups is illustrated in Figure 6(B)–(C).

To detect changes in collagen during liver fibrosis, the expression levels of collagen I in CCl_4 -induced liver tissues treated with different MT preparations were evaluated by immunohistochemical assays. Figure 7(A) showed that the free MT and MT-SLN treatment groups exhibited a slight decrease in collagen I levels compared to the model group, whereas the M6P-HSA-MT-SLN treatment group showed a marked decrease. The analysis of collagen I expression levels in the control, model and different treatment groups is shown in Figure 7(B).

Activation and proliferation of hepatic stellate cells and its excessive secretion of extracellular matrix are important steps in the development of liver fibrosis. As shown in Figure 7(A), the IHC results showed significantly reduced levels of

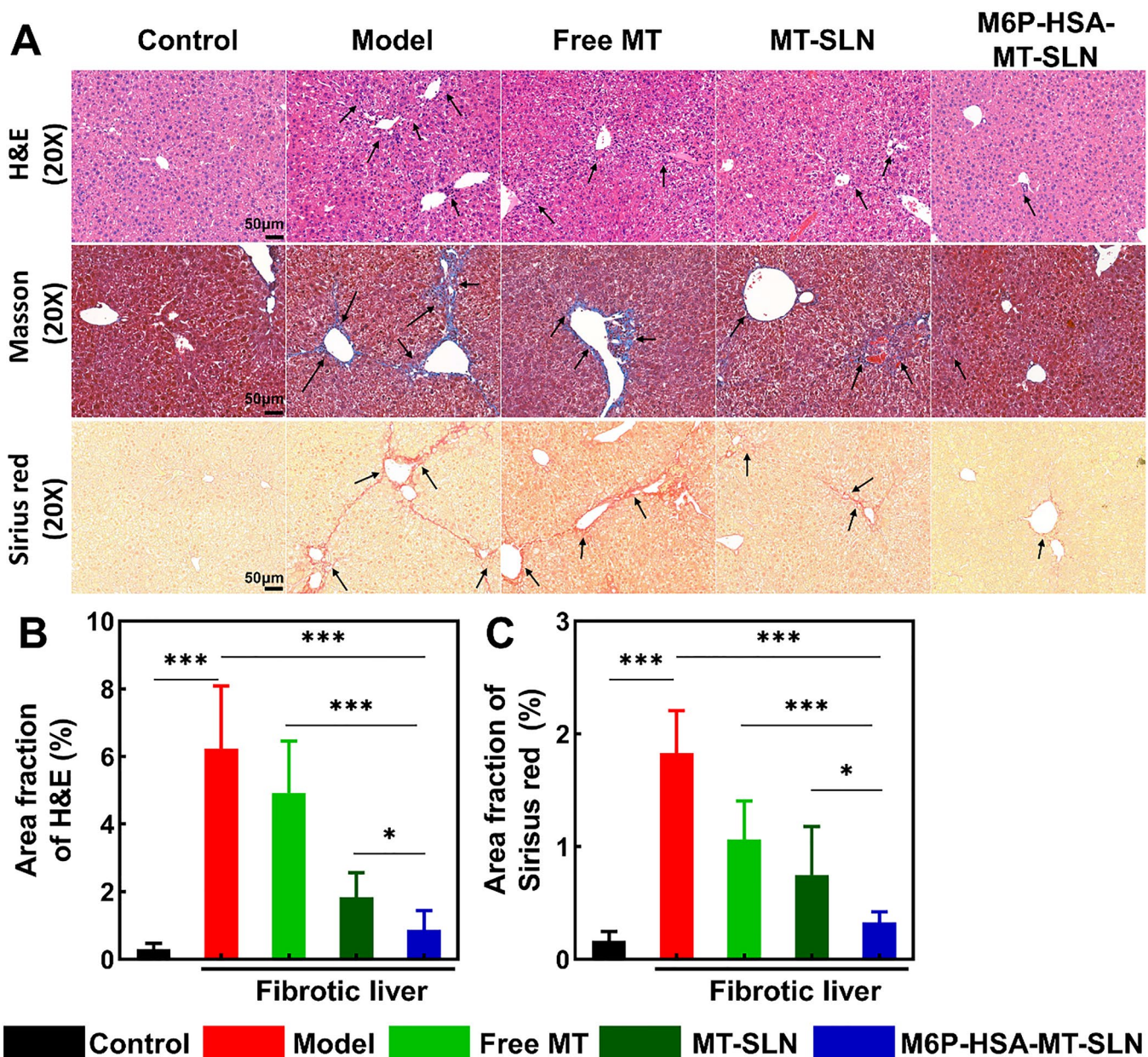


Figure 6. The progression of CCl_4 -induced liver fibrosis was significantly suppressed by M6P-HSA-MT-SLN. (A) Representative images of H&E, Masson and Sirius red-stained liver sections; scale bars are $50\mu\text{m}$. (B) H&E and Sirius red staining quantitative analysis of liver sections. Data represented as mean \pm SD, $n=6$; * $p < 0.05$, ** $p < 0.01$, *** $p < 0.001$.

α -SMA, a marker of hepatic stellate cell activation, in CCl_4 -induced mice treated with M6P-HSA-MT-SLN. In addition, another fibrosis marker, collagen I, also confirmed a remarkable alleviation of liver fibrosis in mice that received M6P-HSA-MT-SLN (Figure 7A,C).

In conclusion, all above results demonstrated that M6P-HSA-MT-SLN significantly inhibited the activation of HSCs and slowed down the progression of liver fibrosis, which may be due to the fact that M6P specifically recognizes HSCs and thus promotes more MT internalization into the cells.

3.8. Biodistribution of MT-SLN and M6P-HSA-MT-SLN

To confirm the targeted delivery efficiency of the designed nanocarriers to the liver, the biodistribution of free MT,

MT-SLN and M6P-HSA-MT-SLN was investigated. Different groups of free MT solution, MT-SLN and M6P-HSA-MT-SLN were administered to fibrotic rats at a concentration of 50 mg/kg body weight. After injection of various MT preparations, mice were anesthetized at specified time points. Blood was drawn from the abdominal aorta, and the liver, spleen, kidneys, lungs, and heart were removed. Figure 8(A)–(E) showed the results of MT concentration-time in each tissue after rat tail vein injection of MT-solution, MT-SLN and M6P-HSA-MT-SLN. After 30 minutes of administration, MT was most distributed in the liver, indicating that MT could be enriched in the liver. Compared with the free MT solution, the accumulation of MT-SLN and M6P-HSA-MT-SLN was higher in the liver, and the content of M6P-HSA-MT-SLN was the highest. After 1 h of administration, the distribution of matrine in the liver and kidney continued to increase and

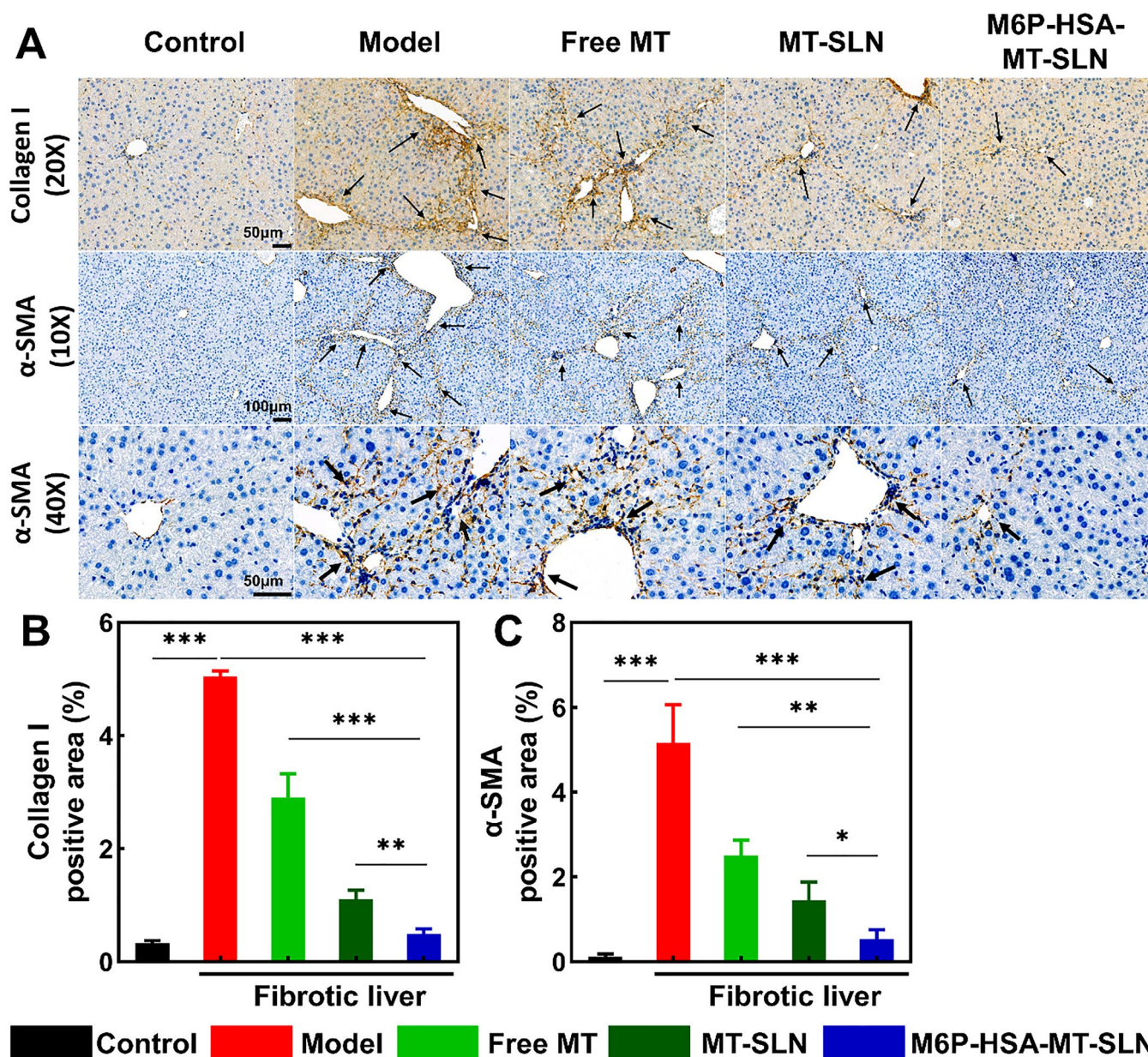


Figure 7. CCl_4 -induced liver fibrosis in mice was alleviated by M6P-HSA-MT-SLN. (A) Images of collagen I and α -SMA immunohistochemical staining of liver sections; scale bars are $50\mu\text{m}$ (collagen I, $20\times$ and α -SMA, $40\times$) and $100\mu\text{m}$ (α -SMA, $10\times$). (B, C) Collagen I and α -SMA immunohistochemical staining quantitative analysis of liver sections. Data represented as mean \pm SD, $n=3$; * $p < 0.05$, ** $p < 0.01$, *** $p < 0.001$.

reached the maximum value. At this time, the concentration of matrine in the liver was $\text{M6P-HSA-MT-SLN} > \text{MT-SLN} > \text{MT}$ solution. Almost 80% of the dose distribution in the organs was taken up by the liver for the M6P-HSA-MT-SLN, which was 1.65- and 1.96-fold higher than the MT-SLN and free MT after 1 h post-injection. After 2h administration, the concentration of MT in various organs in MT solution, MT-SLN and M6P-HSA-MT-SLN gradually decreased, indicating that it was gradually cleared in vivo. During this process, the MT concentration in liver was always higher than other tissues, and the concentration of M6P-HSA-MT-SLN was the highest among three formulations. A small amount of the dose was taken up by the heart, spleen, lung, and kidneys, respectively. The amount of MT in M6P-HSA-MT-SLN taken up by the heart, spleen, lung, and kidney was 1.37-, 0.77-, 0.59-

and 0.93-fold more for MT-SLN and 1.26-, 1.14-, 0.51-, and 0.79-fold more for the free MT-solution.

The change in the time-dependent concentration in the liver change demonstrated that the free MT solution was rapidly distributed and eliminated from the target organ, leaving a relatively low amount in the fibrosis area that was not ideal effect. Conversely, MT-SLN and M6P-HSA-MT-SLN exhibited a high liver concentration and long retention time. In addition, the total amount of M6P-HSA-MT-SLN in the liver from the beginning to 12h was 1.54- and 2.13-folds higher than that of the MT-SLN and free MT solution. These data indicate that M6P-HSA-SLN can effectively increase the MT content in fibrosis liver tissue. In general, these results indicate that the M6P-HSA-MT-SLN can actively target fibrous liver.

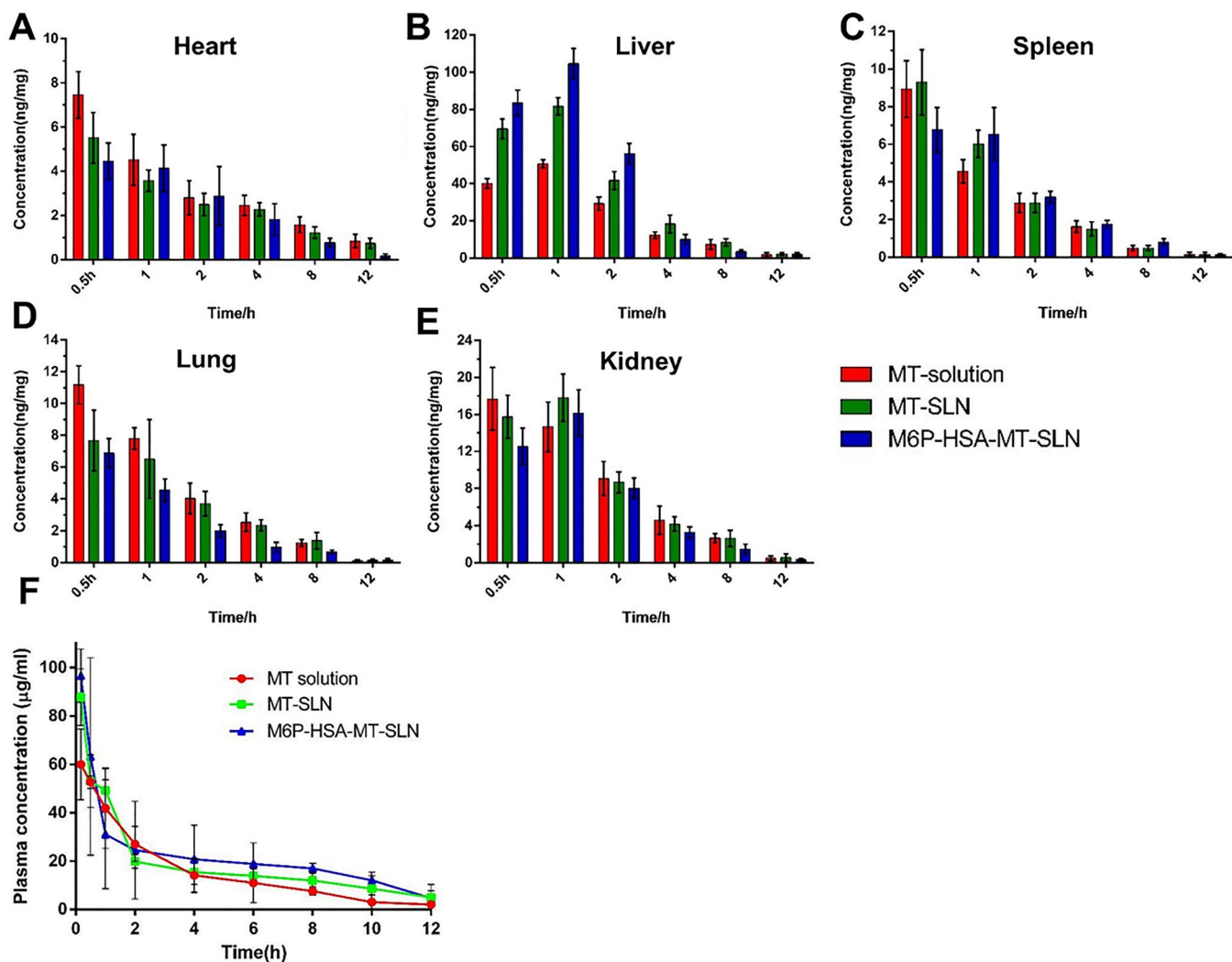


Figure 8. The distribution in main organ and pharmacokinetic study after injection at a dose of 50 mg/kg and the concentration of MT in fibrotic liver. (A-E) The distribution of SLN solution, MT-SLN, and M6P-HSA-MT-SLN in heart, liver, spleen, lung, and kidney. (F) The plasma concentration of MT solution, MT-SLN, and M6P-HSA-MT-SLN in fibrotic mice.

3.9. Pharmacokinetic study

Eighteen healthy male SD rats (200 ± 10 g) were randomly divided into groups A, B and C ($n=6$). Each group was given 50 mg/kg MT solution, MT-SLN and M6P-HSA-MT-SLN, respectively. The Figure 8(F) showed the average drug concentration-time curve of the SD rat intravenous injection of free MT solution, MT-SLN and M6P-HSA-MT-SLN. Compared with MT-solution, the concentration of MT-SLN and M6P-HSA-MT-SLN after administration has decreased rapidly. Within 2 h after administration, the M6P-HSA-MT-SLN and MT-SLN groups in rats were quickly removed, and the concentration of MT in plasma dropped to 18% and 22% of the initial concentration, respectively. However, the MT plasma concentration in the MT-solution maintained at a high level, which is 40% of the initial concentration. The above results show that due to the passive targeting and active targeting capabilities of the liver of MT-SLN and M6P-HSA-MT-SLN, MT was quickly removed in plasma and entered the liver tissue. Over time, the removal rate of MT-SLN and M6P-HSA-MT-SLN is reduced. From 2h to 10h, the plasma concentration of MT-SLN and M6P-HSA-MT-SLN is reduced slowly, which may

be due to MT-SLN and M6P-HSA-MT-SLN have the effects of controlling MT release. In addition, the mean pharmacokinetic parameters for the three preparations were displayed in Table S2, which demonstrating that the area under the curve (AUC) and elimination half-life ($t_{1/2}$) values for M6P-HSA-SLN and HSA-SLN are higher than for free MT free solution. This may be attributed to the fact that the encapsulation of MT by SLN reduces the leakage and degradation of MT in the blood, resulting in a higher blood concentration profile than in the free MT group.

4. Conclusion

In this study, we prepared a liver targeted solid lipid nanoparticle loaded with MT (M6P-HAS-MT-SLN) and evaluated the therapeutic potential of it both in vitro and in vivo. The M6P-HAS-MT-SLN as described previously and allowed a sustained release. MT loaded in M6P-HSA-SLN showed excellent efficacy in alleviating liver fibrosis in vivo. Also, MT was specifically delivered to the liver, resulting in a significant reduction in the serum biomarkers, such as AST, ALT, HA, LN, COL

IV, and PC III. Thus, M6P-HAS-MT-SLN dramatically improved pathophysiological symptoms were detected in the liver fibrosis model mice. The results of the biodistribution studies confirmed that the nanocarrier increases the MT accumulation in the liver for therapeutic efficiency. We anticipate that, in addition to MT, M6P-HSA-SLN nanoparticles can be used to deliver other drugs to the liver for precision treatment of liver fibrosis.

Author contributions

Wensheng Zheng and Yujia Zhang designed the overall project. Xiaochuan Tan mainly carried out all the experiments and wrote the manuscript. Yumei Hao wrote the manuscript and carried out some related experiment. Other authors, such as Nai Ma, Yige Yang, Wenzhen Jin, Ya Meng, Chuchu Zhou participated in some related experiment.

Data availability statement

The data that support the findings of this study are available from the corresponding author upon reasonable request.

Disclosure statement

No potential conflict of interest was reported by the authors.

Ethical approval statement

The authors have adhered to the ARRIVE guidelines. All animal procedures were performed in accordance with the guidelines approved by the Animal Care and Use Committee of the National Institutes for Food and Drug Control (No. 2019 (B) 011) and Institutional Animal Care and Use Committee of the Institute of Materia Medica, Chinese Academy of Medical Sciences and Peking Union Medical College (No. 00007661). Except for the C57 mice and SD rat used in this experiment, other animals cannot effectively construct models and evaluate pharmacodynamics. All animals were housed at $22 \pm 1^\circ\text{C}$, relative humidity $50 \pm 1\%$, and a light/dark cycle of 12/12h. All rats and mice had free access to food and water. Mice were euthanized by intraperitoneal injection of excessive pentobarbital sodium.

Funding

This work was supported by CAMS Innovation Fund for Medical Sciences (CIFMS) (2021-I2M-1-028) and Yunnan Key Laboratory of Southern Medicinal Utilization, Yunnan University of Chinese Medicine (202105AG070012). All animal procedures were carried out under the guidelines approved by the Institutional Animal Care and Use Committee of the Institute of Materia Medica, Chinese Academy of Medical Sciences and Peking Union Medical College.

References

Ban C, Lim S, Chang PS, Choi YJ. (2014). Enhancing the stability of lipid nanoparticle systems by sonication during the cooling step and controlling the liquid oil content. *J Agric Food Chem* 62:1–16.

Bartneck M, Warzecha KT, Tacke F. (2014). Therapeutic targeting of liver inflammation and fibrosis by nanomedicine. *Hepatobiliary Surg Nutr* 36:364–76.

Bataller R, Brenner DA. (2005). Liver fibrosis. *J Clin Invest* 115:209–18.

Batool S, Zahid F, Ud-Din F, et al. (2021). Macrophage targeting with the novel carbopol-based miltefosine-loaded transfersomal gel for the

treatment of cutaneous leishmaniasis: in vitro and in vivo analyses. *Drug Dev Ind Pharm* 47:440–53.

Beljaars L, Molema G, Weert B, et al. (1999). Albumin modified with mannose 6-phosphate: a potential carrier for selective delivery of antifibrotic drugs to rat and human hepatic stellate cells. *Hepatology* 29:1486–93.

Byass P. (2014). The global burden of liver disease: a challenge for methods and for public health. *BMC Med* 12:159.

Dai ZJ, Gao J, Ji ZZ, et al. (2009). Matrine induces apoptosis in gastric carcinoma cells via alteration of Fas/FasL and activation of caspase-3. *J Ethnopharmacol* 123:91–6.

Din FU, Mustapha O, Kim DW, et al. (2015). Novel dual-reverse thermo-sensitive solid lipid nanoparticle-loaded hydrogel for rectal administration of flurbiprofen with improved bioavailability and reduced initial burst effect. *Eur J Pharm Biopharm* 94:64–72.

Din F. u, Zeb A, Shah KU, Zia Ur R. (2019). Development, in-vitro and in-vivo evaluation of ezetimibe-loaded solid lipid nanoparticles and their comparison with marketed product. *J Drug Delivery Sci Technol* 51:583–90.

Feng Y, Ying HY, Qu Y, et al. (2016). Novel matrine derivative MD-1 attenuates hepatic fibrosis by inhibiting EGFR activation of hepatic stellate cells. *Protein Cell* 7:662–72.

Gonzalo T, Talman EG, van de Ven A, et al. (2006). Selective targeting of pentoxifylline to hepatic stellate cells using a novel platinum-based linker technology. *J Control Release* 111:193–203.

Greupink R, Bakker HI, Bouma W, et al. (2006). The antiproliferative drug doxorubicin inhibits liver fibrosis in bile duct-ligated rats and can be selectively delivered to hepatic stellate cells in vivo. *J Pharmacol Exp Ther* 317:514–21.

Greupink R, Bakker HI, Reker-Smit C, et al. (2005). Studies on the targeted delivery of the antifibrogenic compound mycophenolic acid to the hepatic stellate cell. *J Hepatol* 43:884–92.

Hagens WI, Olinga P, Meijer DK, et al. (2006). Gliotoxin non-selectively induces apoptosis in fibrotic and normal livers. *Liver Int* 26:232–9.

Jiang JH, Pi J, Jin H, et al. (2018). Chinese herb medicine matrine induce apoptosis in human esophageal squamous cancer KYSE-150 cells through increasing reactive oxygen species and inhibiting mitochondrial function. *Pathol Res Pract* 214:691–9.

Jin W, Xu P, Zhan Y, et al. (2007). Degradable cisplatin-releasing core-shell nanogels from zwitterionic poly(beta-aminoester)-graft-PEG for cancer chemotherapy. *Drug Deliv* 14:279–86.

Kisseleva T, Brenner DA. (2008). Mechanisms of fibrogenesis. *Exp Biol Med (Maywood)* 233:109–22.

Kong WH, Park K, Lee MY, et al. (2013). Cationic solid lipid nanoparticles derived from apolipoprotein-free LDLs for target specific systemic treatment of liver fibrosis. *Biomaterials* 34:542–51.

Kumar S, Randhawa JK. (2013a). Preparation and characterization of Paliperidone loaded solid lipid nanoparticles. *Colloids Surf B Biointerfaces* 102:562–8.

Kumar S, Randhawa JK. (2013b). High melting lipid based approach for drug delivery: solid lipid nanoparticles. *Mater Sci Eng C Mater Biol Appl* 334:1842–52.

Li W, Zhou C, Fu Y, et al. (2020). Targeted delivery of hyaluronic acid nanomicelles to hepatic stellate cells in hepatic fibrosis rats. *Acta Pharm Sin B* 10:693–710.

Luk JM, Zhang QS, Lee NP, et al. (2007). Hepatic stellate cell-targeted delivery of M6P-HSA-glycyrrhetic acid attenuates hepatic fibrogenesis in a bile duct ligation rat model. *Liver Int* 27:548–57.

Ma L, Wen S, Zhan Y, et al. (2008). Anticancer effects of the Chinese medicine matrine on murine hepatocellular carcinoma cells. *Planta Med* 74:245–51.

Mahdinloo S, Hemmati S, Valizadeh H, et al. (2022). Synthesis and preparation of vitamin A coupled butein-loaded solid lipid nanoparticles for liver fibrosis therapy in rats. *Int J Pharm* 625:122063.

Mederacke I, Hsu CC, Troeger JS, et al. (2013). Fate tracing reveals hepatic stellate cells as dominant contributors to liver fibrosis independent of its aetiology. *Nat Commun* 4:2823.

Mirchandani Y, Patravale VB, S B. (2021). Solid lipid nanoparticles for hydrophilic drugs. *J Control Release* 335:457–64.

- Rahman HS, Rasedee A, How CW, et al. (2013). Zerumbone-loaded nanostructured lipid carriers: preparation, characterization, and antileukemic effect. *Int J Nanomedicine* 8:2769–81.
- Rana I, Khan N, Ansari MM, et al. (2020). Solid lipid nanoparticles-mediated enhanced antidepressant activity of duloxetine in lipopolysaccharide-induced depressive model. *Colloids Surf B Biointerfaces* 194:111209.
- Sakaida I, Terai S, Yamamoto N, et al. (2004). Transplantation of bone marrow cells reduces CCl₄-induced liver fibrosis in mice. *Hepatology* 40:1304–11.
- Song K, Hao Y, Tan X, et al. (2023). Microneedle-mediated delivery of Ziconotide-loaded liposomes fused with exosomes for analgesia. *J Control Release* 356:448–62.
- Xing R, Mustapha O, Ali T, et al. (2021). Development, characterization, and evaluation of SLN-loaded thermoresponsive hydrogel system of topotecan as biological macromolecule for colorectal delivery. *Biomed Res Int* 2021:9968602.
- Xu Z, Chen L, Gu W, et al. (2009). The performance of docetaxel-loaded solid lipid nanoparticles targeted to hepatocellular carcinoma. *Biomaterials* 30:226–32.
- Xu X, Zhao C, Yang H, et al. (2011). Anti-inflammatory activity of injectable dexamethasone acetate-loaded nanostructured lipid carriers. *Drug Deliv* 18:485–92.
- Yang B, Jiang J, Jiang L, et al. (2020). Chitosan mediated solid lipid nanoparticles for enhanced liver delivery of zedoary turmeric oil in vivo. *Int J Biol Macromol* 149:108–15.
- Zhang JP, Min Z, Jin C. (2001). Matrine inhibits production and actions of fibrogenic cytokines released by mouse peritoneal macrophages. *Acta Pharmacol Sin* 228:765–8.
- Zhang Y, Zhang N, Song H, et al. (2019). Design, characterization and comparison of transdermal delivery of colchicine via borneol-chemically-modified and borneol-physically-modified ethosome. *Drug Deliv* 26:70–7.